Synthesis of Modified Silica Spheres Used for the Preparation of Dual Ultraviolet- and Thermo-Cured Epoxyacrylate/Silica Composites

Yu-Chieh Su, Liao-Ping Cheng, Trong-Ming Don
Department of Chemical and Materials Engineering, Tamkang University, New Taipei City 25137, Taiwan

To investigate the interfacial effect on properties of epoxyacrylate–silica composites, submicron-sized silica spheres were synthesized by sol–gel reaction under a basic environment and their surfaces were endowed with vinyl functional groups by further modification with 3-methacryloxypropyl trimethoxy silane. The pure silica (PS) and the modified silica (MPS) spheres were characterized by Fourier transform infrared, ^{29}Si- and ^{13}C-nuclear magnetic resonance (NMR), scanning electron microscope (SEM), and particle size analyzer. The silica spheres were then added to the presynthesized difunctional epoxyacrylate resin with one vinyl group and one epoxide group at each end, in addition to the photo- and thermo-curing agents. After cure, thermal and mechanical properties of the obtained epoxyacrylate–silica composites were measured and compared. Tensile mechanical properties including initial modulus, ultimate tensile strength, and elongation at break, as well as the fracture energy of the epoxyacrylate–silica composite were all increased by increasing the content of silica spheres. Moreover, the composites filled with MPS had stronger interfacial strength between silica sphere and matrix than those with PS and thus exhibited an additional increase of tensile mechanical properties and fracture toughness. The increase of fracture toughness was owing to the crack deflection and particle–matrix debonding as evidenced by SEM pictures on the fracture surface. POLYM. ENG. SCI., 52:2462–2472, 2012. © 2012 Society of Plastics Engineers

INTRODUCTION

Epoxy resins are commercially used in many applications, including surface coatings, structural adhesives, packaging of electronic products, and matrix for composite materials [1, 2]. Through the proper selection of resin and curing agent, the cured epoxy resins exhibit many desirable properties, such as low cure shrinkage, low creep, excellent adhesive strength, good chemical resistance, high mechanical strength, good thermal stability, and excel-

lent electrical insulation [3]. Especially, the demand of epoxy resins has rapidly grown for industrial applications in the electronic products, such as the molding compounds used for the encapsulation of integrated circuit chips and the epoxy composites for printed circuit boards [4, 5]. However, the high-performance epoxy resin suffers from the problems of high curing temperature and long curing time. To solve these problems, ultraviolet (UV)-curable resins are often employed and the most used one is known to be the epoxyacrylate. Commercial epoxyacrylate is generally produced and used in the form of bisacrylate-terminated epoxy resin, also called vinyl ester resin [6, 7]. This resin has some advantageous properties including excellent reactivity owing to the two unsaturated end groups, and thus can be rapidly cured by UV light [8, 9]. Instead of using bisacrylate-terminated epoxy resin, a difunctional epoxyacrylate oligomer with a vinyl group at one end and an epoxide group at the other end, or called monoacrylate-terminated epoxy resin, was synthesized in this study for the later preparation of epoxyacrylate–silica composites, because it can be applied in an UV-curing and/or thermo-curing processes, making it especially useful as an adhesive sealant for liquid crystal display manufacturing [10].

The structure of thermosetting epoxy resins has also an unsatisfactory drawback in that they are relatively brittle, with a poor resistance to crack initiation and growth. Nevertheless, it has been well established for many years that the toughness of an epoxy resin incorporated with a second microphase of a dispersed rubber or a thermoplastic polymer can be improved [11]. Unfortunately, the presence of the low-modulus rubbery phase typically increases the viscosity of the system before cure and reduces the modulus and the glass transition temperature of the cured epoxy. Hence, rigid inorganic particles have been tested to increase the modulus and toughness, and hopefully not to substantially affect the thermal properties of the epoxy resin. Several studies indicated that the modulus, strength, and toughness can be simultaneously increased with the addition of nanoscale fillers. Rosso et al. [12] incorporated nanosilica particles (below 50 nm) to diglycidyl ether of bisphenol-A (DGEBA)-based epoxy resin to prepare epoxy–silica nanocomposite (ESN). They
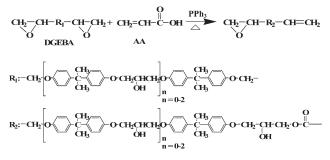
found that with the addition of 5 vol% nanosilica, the relative improvement in Young's modulus ($E_{ESN}/E_{neat\ resin}$) was about 1.22 and the fracture toughness (K_{Ic}) was increased by more than 70%, compared to the neat epoxy. Unfortunately, the glass transition temperature still decreased from 95 to 89°C. Liang and Pearson [13] added two types of nanosilica (20 and 80 nm) to prepare ESNs. The compressive modulus of ESNs moderately increased with the amount of nanosilica, and the relative improvement in compressive modulus reached 1.2 when the nanosilica content was added up to 17.4 vol%. Moreover, they found that the ESNs filled with nanosized silica had higher toughness than the epoxies filled with the micron-sized glass spheres (mean diameter, 42 μm). The increase in toughness was attributed to the zone-shielding mechanism involving matrix plastic deformation. Johnsen et al. [14] also added nanosized silica (20 nm) into the DGEBA-based epoxy resin. After thermal cure at 90°C for 1 h and then at 160°C for 2 h, the relative improvement on Young's modulus of the formed ESN containing 9.6 vol% silica was about 1.22. The fracture toughness (K_{Ic}) and fracture energy (G_{Ic}) of ESN with 7.1 vol% silica content could be increased by 100 and 233%, respectively. They believed that the toughening mechanism of ESNs involved the plastic void growth around debonded particles.

The nanoscaled silica particles used in the aforementioned ESNs were produced by the sol–gel technique. This technique also provides a simple way for the surface modification of the nanoparticles to avoid their agglomeration at a higher degree of filling and to adjust the interfacial compatibility with the polymer matrix [15]. Chan et al. [16] found that modification of silica surface during silanization could improve the fracture toughness of nanocomposites owing to the increase of interfacial bonding. Compared to the mechanical dispersing technique for silica-based nanoparticles, the sol–gel technique is a very efficient chemical method for embedding agglomerate-free silica particles in epoxy resins [17]. However, only few studies [18–20] have been done on the preparation and characterization of epoxy composites incorporated with submicron-sized silica spheres (100 nm^{-1} μm). In this study, submicron-sized silica spheres were prepared by the sol–gel reaction from tetraethyl orthosilicate (TEOS) in a basic environment and their surfaces were further modified with 3-methacryloxypropyl trimethoxy silane (MPTMS). The prepared silica spheres with and without vinyl functional groups on surface were then added into the presynthesized difunctional epoxyacrylate resin. After UV- and thermo-curing, thermal and mechanical properties of the cured epoxyacrylate resins were measured and the effects of the added silica spheres on the properties, especially fracture toughness, were thus investigated.

EXPERIMENTAL

Material

The difunctional epoxyacrylate resin having one epoxide end group and one vinyl group at the other end was
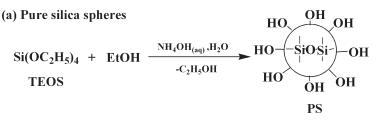

SCHEME 1. °Synthesis of difunctional epoxyacrylate under a temperature profile of 100°C for 2 h and another 2 h at 120°C. PPh$_3$ is TPP.
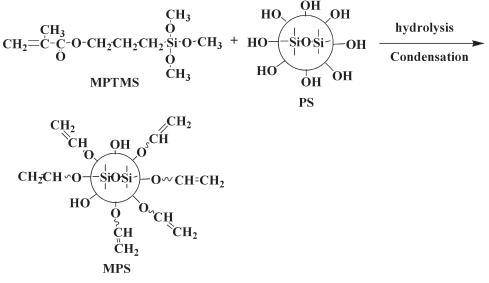
synthesized from the DGEBA and acrylic acid (AA) under a suitable reaction condition [21]. Briefly, DGEBA and AA with an equivalent ratio of 2 were charged into the reactor, and the reaction was catalyzed by triphenylphosphine (TPP) under a temperature profile of 100°C for 2 h and another 2 h at 120°C. The addition esterification of the epoxide group with the carboxyl group catalyzed by TPP is shown in Scheme 1. TEOS, MPTMS, and ammonia (25% in water) were purchased from Acros (Geel, Belgium). 2-Benzyl-2-dimethylamino-1-(4-morpholinophenyl)-butanone-1, also called I-369, and 2-isopropyl thioxanthone, also called ITX, from Ciba were used as the photo initiator and accelerator, respectively. Imidazole (C11Z-A) from Shikoku Chemicals (Tokyo, Japan) was used as the thermal curing agent. Trimethylolpropane triacrylate (TMPTA) as a reactive diluent was purchased from Acros (Geel, Belgium).

Preparation of Colloidal Silica Spheres

The submicron-sized silica spheres were prepared in ethanol according to the process developed by Stöber et al. [22] with a slight modification. In a typical procedure, aqueous ammonia (25%), water, and ethanol were all added into an Erlenmeyer flask under continuous stirring at room temperature. The amounts of ethanol and water were fixed at 1600 and 128 mL, respectively, and the amount of aqueous ammonia was changed from 24 to 80 mL to obtain silica spheres with different sizes. The TEOS (96 mL) was added to the solution for the sol–gel reaction. After 30 min of prereaction, MPTMS with a molar ratio of 1:1 to the TEOS was added into the solution drop-by-drop, and the reaction was allowed to continue for additional 23.5 h with stirring to obtain modified silica (MPS) spheres. For the preparation of pure silica (PS) spheres, the total reaction time was kept at 24 h without the addition of MPTMS. The reactions are shown in Scheme 2. The prepared sol was centrifuged (9000 rpm, 13 × 10^3 rcf) to separate the silica particles. These particles were redispersed in ethanol by sonication and centrifuged again. The final silica particles were then dried at 60°C for 24 h. The dried particles were easily redispersed by sonication in ethanol or acetone. The yield was in the range between 95 and 98% for the PS spheres.

(a) Pure silica spheres

$$Si(OC_2H_5)_4 \ + \ EtOH \xrightarrow[\substack{-C_2H_5OH}]{NH_4OH_{(aq)}, H_2O}$$

TEOS

HO, OH, OH

HO—SiOSi—OH

HO, OH, OH

PS

(b) Surface modifiction of silica spheres

$$CH_2=\overset{\overset{\displaystyle CH_3}{|}}{C}-\overset{\overset{\displaystyle}{||}}{\underset{\displaystyle O}{C}}-O-CH_2CH_2CH_2\overset{\overset{\displaystyle CH_3}{|}}{\underset{\displaystyle \underset{\displaystyle CH_3}{O}}{Si}}-O-CH_3 \ + $$

MPTMS

HO, OH, OH

HO—SiOSi—OH

HO, OH, OH

PS

$$\xrightarrow[\text{Condensation}]{\text{hydrolysis}}$$

CH$_2$
CH   OH   CH$_2$
O   O   CH
CH$_2$CH O—SiOSi—O CH=CH$_2$
HO   O   O CH
CH   CH$_2$
CH$_2$

MPS

SCHEME 2.   °Preparation of (a) PS spheres, (b) surface-MPSs.

Yet, for the preparation of MPS spheres, the yield was decreased to about 30–40%.

Preparation of Epoxyacrylate–Silica Composites

The epoxyacrylate–silica composites were prepared by mixing difunctional epoxyacrylate oligomer, silica spheres, reactive diluent, photo initiator, and thermal-curing agent. The dried silica spheres were first dispersed by sonication in acetone and then mixed with the epoxyacrylate resin. The loading concentrations of silica spheres were 5, 10, 15, and 20 phr (parts per hundred parts of epoxyacrylate resin). After removing the solvent, the photo initiator (I-369) and its accelerator (ITX), thermal-curing agent (C11Z-A), and reactive diluent (TMPTA) were all added to the epoxyacrylate–silica mixture. The total concentration of I-369 and ITX was 3.85 phr and the weight ratio of I-369 to ITX was controlled at 5:1. The concentrations of the curing agent (C11Z-A) and the reactive diluent (TMPTA) were 3.85 and 23 phr, respectively. The mixture was poured into an uncovered Teflon mould and then cured by UV irradiation (140 mJ/cm^2) followed by thermal cure for 2 h at 150°C.

Characterizations

Structure analyses of the silica spheres (PS and MPS) were carried out using the Fourier transform infrared (FTIR) spectrophotometer (Magna-IR spectrometer 550, Nicolet, USA). Sample was ground into powder, mixed with potassium bromide (KBr), and then pressed into a transparent disc. The recorded wave number range was from 4000 to 400 cm^{-1} with a resolution of 4 cm^{-1}. Chemical structures of the silica spheres were also analyzed with a nuclear magnetic resonance (NMR) technique (Bruker DSX400WB NMR). Solid ^{29}Si- and ^{13}C-NMR spectra were obtained at a frequency of 79.49 MHz for ^{29}Si and 100.61 MHz for ^{13}C. Experiments were performed with a Bruker 7-mm wide-bore MAS probe. The MAS spinning speed was 5 kHz, and the 90° pulse time was 5.5 μs. The chemical shifts were expressed in ppm with respect to tetramethylsilane.

The size and size distribution of silica spheres were determined at 20°C by the dynamic light scattering method, using Zetasizer Malvern DTS 1060. The instrument employed a monochromatic coherent helium-neon laser (633 nm) as the light source. A 4-mL sol sample was injected into the quartz cuvette and the scattered light was recorded at 173° with respect to the incident light.

The texture of silica spheres and fracture surface of epoxyacrylate composites were examined by a scanning electron microscope (FESEM, Leo1530, Germany). To observe dispersive particles, a drop of dilute silica sol was placed on a glass slide and air-dried afterward. All specimens were sputtered with Pt in approximately 3-nm thickness to increase conductivity.

Mechanical Properties

Tensile mechanical properties: initial modulus (E), ultimate tensile strength (σ_b), and elongation at break (ε_b) were measured by using a universal testing machine (Model AGS-J, Shimadzu, Japan). The specimens with a thickness of 1 mm were prepared based on the ASTM standard D638. The test speed was kept at 0.5 mm/min. Five specimens were tested for each condition and the results were then averaged.

The single-edge-notch bending (SENB) test was used to determine the fracture toughness, K_{Ic}, according to ASTM D5045. At least, five specimens for each formulation were tested. The value of the fracture energy, G_{Ic}, was calculated using *Eq. 1*,

$$G_{Ic} = \frac{K_{Ic}^2}{E}\left(1 - v^2\right) \qquad (1)$$

where E is the modulus of elasticity estimated from the tensile test, and v is the Poisson's ratio of epoxy, taken as 0.35.

Thermal Properties

A differential scanning calorimeter (DSC, TA 2920 from TA Instruments) was used to record the thermograms of epoxyacrylate–silica composites after cure. Samples (8–10 mg) were first heated up to 210°C and held at that temperature for 1 min under a nitrogen atmosphere. Then, they were cooled down to −10°C at a cooling rate of 20°C/min and then reheated up to 210°C at a heating rate of 20°C/min. The second heating curve was used to determine the T_g.

The thermal expansion coefficients of the cured epoxyacrylates were determined by a thermal mechanical analyzer (TMA Q400, TA Instruments). The thermal expansion coefficients before and after the glass transition (α_1 and α_2, respectively) were obtained by the measurement of the linear dimensional variations with temperatures. The T_g of a sample was identified as the intercept of the two tangent lines at which a change in slope occurred, that is, above and below T_g. Samples were heated from 30 to 200°C with a scanning rate of 10°C/min in the nitrogen atmosphere.

RESULTS AND DISCUSSION

Structure Analysis and Morphology of MPS Spheres

Uniform silica spheres were prepared following the well-known Stöber–Fink–Bohn method [22] with a slight modification, where hydrolysis and condensation of alkoxysilanes were catalyzed by ammonia in a mixture of ethanol, aqueous ammonia, and water. Formation of spherical particles was the result of a complex mechanism of nucleation and growth. Reactions (a) and (b) in Scheme 2 describe the synthesis of PS and MPS spheres by hydrolysis and condensation of alkoxysilanes in the basic environment. FTIR spectra for the prepared PS and MPS are
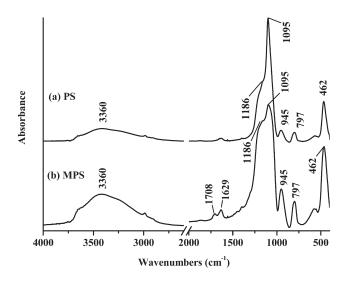

FIG. 1. FTIR spectra of (a) unmodified silica spheres (PS) and (b) MPS spheres.

shown in Fig. 1. The broad absorption band centered at 3360 cm^{-1} is owing to OH stretching of various Si—OH groups on PS and MPS. In addition, the absorption peak at 945 cm^{-1} is also caused by the Si—OH group (Si—O—stretching). The absorption peaks at about 797 and 1095 cm^{-1} are caused by Si—O—Si symmetric and asymmetric stretching vibration, respectively, indicating the generation of Si—O—Si in the system [23]. The peak of the Si—O—Si asymmetric stretching vibration is usually split by long-range coupling Coulomb interactions into two components: a transverse optical (TO) and a longitudinal optical (LO) component. The peak near 1095 cm^{-1} has been generally related to the TO component; whereas the shoulder at 1186 cm^{-1} under the peak of 1095 cm^{-1} is referred to the LO component [24]. The absorption peak at about 462 cm^{-1} is caused by Si—O—Si bending vibration. Compared to Fig. 1a, the band centered at 1095 cm^{-1} becomes broader when the silica was modified with MPTMS, as shown in Fig. 1b. This is owing to the overlap of Si—O—Si (1000–1100 cm^{-1}), Si—O—C (1080–1120 cm^{-1}) and C—O—C (1000–1300 cm^{-1}), where the latter two come from the MPTMS segments. Figure 1b also shows the carbonyl (C═O) stretching band at 1708 cm^{-1} and the vinyl (C═C) stretching band at 1629 cm^{-1}, further validating the successful bonding of vinyl group on silica spheres by reaction with MPTMS.

Further investigation of the chemical structure of the silica spheres was carried out by solid-state ^{29}Si-NMR analysis. According to the nomenclature suggested in the literature [25–27], M, D, T, and Q structures correspond to one, two, three, and four Si—O— bridges, respectively. In the symbol of M^n, D^n, T^n, and Q^n, n refers to the number of —O—Si[tbond] groups bonded to the silicon atom. Taking code Q as an example, a unit with two —OH groups is assigned as Q^2: (HO)$_2$Si(—OSi[tbond])$_2$, with one —OH group as Q^3: (HO)$_1$Si(—OSi[tbond])$_3$, and with no —OH group as Q^4: Si(—OSi[tbond])$_4$. T^n
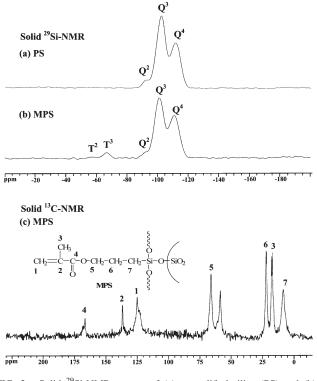
FIG. 2. Solid ^{29}Si-NMR spectra of (a) unmodified silica (PS) and (b) MPS by MPTMS. (c) Solid ^{13}C-NMR spectrum of MPS by MPTMS.

structures have one organic side group (Si—R) and three Si—O— units. Therefore, T^1 is $(HO)_2Si(R)(—OSi[tbond])$, T^2 is $(HO)_1Si(R)(—OSi[tbond])_2$, and T^3 is $Si(R)(—OSi[tbond])_3$. It is easy to differentiate among Q^4, Q^3, and Q^2, because their chemical shifts lie approximately 10 ppm apart. The transformation of a Q structure into a T structure causes a shift of about 45 ppm and again there is a separation of approximately 10 ppm between the silicon in T^3, T^2, and T^1. The ^{29}Si-NMR spectrum of the PS spheres, Fig. 2a, shows three signals at −93 (Q^2), −101 (Q^3), and −111 (Q^4) ppm, which are usually assigned to geminal silanol groups, free silanol groups, and siloxane bonds without hydroxyl groups, respectively [28, 29]. After modification with MPTMS having one organic side group, Fig. 2b shows that the MPS not only have Q^2, Q^3, and Q^4 structures, but also have two additional silicon atoms at −57 and −67 ppm designated as T^2 and T^3 structures, respectively. As expected, the grafting process reduces the intensities of the signals of geminal and free silanol groups in the respective Q^2 and Q^3 in comparison with that of the siloxane group in Q^4. Therefore, the peaks observed in the range from −50 to −80 ppm prove that the silica surface was chemically grafted with MPTMS and thus had vinyl functional groups on it.

The organic functional group bonded to the silica surface was further confirmed by solid-state ^{13}C-NMR spectra. Figure 2c shows the solid-state ^{13}C-NMR spectrum of the MPS. The carbons of MPTMS on the silica surface could be easily identified according to their chemical

shifts. In addition to the $\underline{C}\!=\!\underline{C}$ absorption peaks at 125.3 and 137.0 ppm (indicated as 1 and 2 in the spectrum), the spectrum of MPS exhibits the absorption peaks at 17.6 and 116.9 ppm which are caused by $\underline{C}H_3$ and $\underline{C}\!=\!O$ attached to the C=C bond (indicated as 3 and 4 in the spectrum), respectively. The peaks at 66.5, 22.5, and 8.9 ppm are assigned to the propoxyl group, indicated as 5, 6, and 7 in the spectrum. An additional peak at about 59.0 ppm is found, which is possible caused by the unhydrolyzed ethoxy group of TEOS and/or the residual ethanol solution trapped inside the silica particles [30]. Nevertheless, the results of ^{13}C-NMR spectra indicate the successful bonding of vinyl group on silica spheres by reaction with MPTMS, in accordance with the ^{29}Si-NMR and FTIR analyses.

Figure 3 shows the SEM pictures of silica spheres that were purified by centrifugation and washing, and then redispersed by sonication in ethanol. The sample was prepared by dispensing one drop of the suspension onto a glass slide. It was allowed to dry at room temperature and then sputtered with Pt. The SEM picture of PS spheres prepared by adding 48 mL of $NH_4OH_{(aq)}$ into the ethanol solution is shown in Fig. 3a. It was found that the spherical particles obtained were highly uniform in size and without any aggregation. The average particle size was 400 ± 10 nm based on 50 measured particles. In addition, the surface of silica spheres was smooth and featureless.
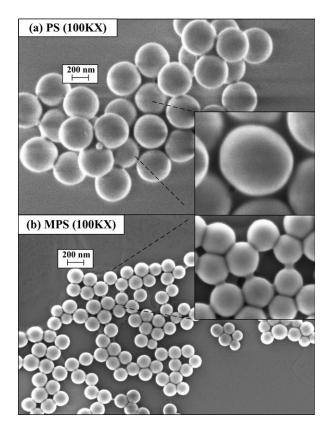

FIG. 3. SEM images of (a) unmodified silica spheres (PS) with an average particle size of 400 ± 10 nm, and (b) MPS spheres with an average particle size of 170 ± 30 nm. For both systems, $EtOH/H_2O/NH_4OH_{(aq)} = 1600/128/48$ mL.
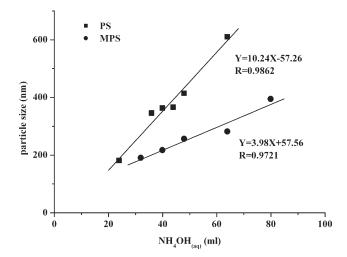
FIG. 4. The changes of particle size of PS and MPS spheres with the added amount of ammonia$_{(aq)}$ in the sol–gel reaction, while the EtOH and H$_2$O were kept at 1600 and 128 mL, respectively. The particle size was measured by dynamic light scattering.

In contrast, Fig. 3b shows that the surface of MPS spheres prepared with the same conditions was slightly rougher than that of PS spheres. In addition, bridging was observed among particles. Bridging occurred during the evaporation of the solvent because MPTMS not only was chemically bonded to the particle surface, but also exhibited strong hydrophobic interactions via its alkyl groups. In addition, MPTMS also played the role of an inhibitor for particle growth owing to less condensation and steric hindrance that could cause the particle size to be smaller and less uniform (170 ± 30 nm).

The Effect of Ammonia on the Particle Size of Silica Spheres

The prepared colloidal silica spheres were further characterized by dynamic light scattering. Many researchers have already reported that the size and uniformity of the resultant silica particles are greatly affected by the concentrations of TEOS, water, and catalyst, as well as the type of solvent, etc. [31–33]. In this study, the effect of the added amount of base-catalyst (NH$_4$OH$_{(aq)}$) on the particle size of silica was also investigated. Figure 4 shows the changes in particle diameter (nm) with the added amount of aqueous ammonia (25%), whereas the amounts of all other components were kept constant. A linear relationship of the particle diameter with the added amount of aqueous ammonia was obtained. The particle size of PS spheres could be controlled in the range of 150–600 nm. For the modified silica particles, the size was smaller under the same reaction conditions, between 150 and 400 nm, because the MPTMS inhibited the growth of particles.

Tensile Mechanical Properties of the Epoxyacrylate–Silica Composites

The silica spheres with different sizes from 150 to 400 nm were added to the difunctional epoxyacrylate oligomer together with the photo- and thermo-initiators as well as the reactive diluent to prepare epoxyacrylate–silica composites. After UV- and thermal-cure, both conversions of C=C double bond and epoxide group were >98% as demonstrated by FTIR spectra. Tensile mechanical properties of the obtained composites were then determined by a tensile test instrument. It was found that the particle size of silica spheres, ranging from 150 to 400 nm, did not significantly affect the tensile mechanical properties for composites with the same amount of silica particles (data not shown). That is, small changes in particle size would not affect the tensile mechanical properties of epoxyacrylate–silica composite. Recently, some studies also showed that the initial modulus of polymer composites filled with micronsized or nanosized spheres was mainly affected by the filler volume fraction and Young's moduli of the filler and polymer matrix, but not the size of the filler [13, 34]. In the following experiments, the silica spheres with particle size about 170 nm were chosen to be incorporated into the epoxyacrylate to investigate the effect of the silica content on the mechanical and thermal properties of the epoxyacrylate composite.

The tensile mechanical properties of epoxyacrylate–silica composites are summarized in Table 1. A tensile modulus of 2.63 GPa was measured for the cured neat epoxyacrylate resin (EA). The modulus was found to increase by the addition of silica spheres, as shown in Fig. 5. The increase in modulus is expected because the modulus of silica is much higher than that of the epoxyacrylate matrix. In addition, it was found that the extent of increase was more evident for the epoxyacrylate loaded with MPS (EA–MPS) than with the same amount of PS (EA–PS). The relative improvement in tensile modulus ($E_{EA–MPS}/E_{EA}$) reached 1.24 when the MPS content was 20 phr (equivalent to 9.46 vol%). This improvement in modulus is better than the results reported by Liang and Pearson [13] and Johnsen et al. [14] for the composites with the same volume fraction of silica, because the MPS had surface vinyl functional groups that could form chemical bonding between the particles and the matrix and thus increase their interfacial strength.

The measured moduli of composites can be compared to the theoretical predictions. These are many models that can be used to predict the moduli of epoxyacrylate–silica composites. In the present study, two quantitative models, Halpin–Tsai and Lewis–Nielsen model were adopted, as shown in Fig. 5. Halpin–Tsai model [35] is a theoretical model commonly used to predict the increase of Young's modulus with respect to the polymer matrix in organic–inorganic composites. The predicted composite's modulus is calculated according to *Eq. 2*,

$$E_c = \frac{1 + \zeta \eta V_f}{1 - \eta V_f} E_m \quad \eta = \frac{\left(\frac{E_f}{E_m} - 1\right)}{\left(\frac{E_f}{E_m} + \zeta\right)} \quad (2)$$

where E_c, E_m, and E_f are Young's moduli of the composite, the polymer matrix, and the particle filler, respectively; V_f is the volume fraction of the particles, and ζ is

TABLE 1. Tensile mechanical properties including initial modulus (E), ultimate tensile strength (σ_b), and elongation at break (ϵ_b) and fracture toughness of epoxyacrylate–silica composites with different silica contents.

| Sample[a] | Silica content | | E (GPa) | σ_b (MPa) | ε_b (%) | K_{Ic} (MPa m$^{1/2}$) | G_{Ic} (J/m^2) |
	Weight (phr)	Volume[b] (%)					
EA	0	0	2.63 ± 0.10^c	34.8 ± 3.8	1.42 ± 0.12	0.66 ± 0.11	145 ± 51
EA–PS5	5	2.55	2.79 ± 0.08	54.3 ± 2.2	2.28 ± 0.15	0.94 ± 0.03	280 ± 17
EA–PS10	10	4.96	2.88 ± 0.05	56.8 ± 2.4	2.23 ± 0.12	1.05 ± 0.02	336 ± 11
EA–PS15	15	7.27	2.99 ± 0.07	66.3 ± 3.4	2.41 ± 0.07	1.22 ± 0.03	439 ± 19
EA–PS20	20	9.46	3.07 ± 0.07	62.4 ± 4.2	2.48 ± 0.38	1.29 ± 0.08	483 ± 58
EA–MPS5	5	2.55	2.75 ± 0.10	58.9 ± 5.0	2.32 ± 0.27	1.02 ± 0.12	332 ± 84
EA–MPS10	10	4.96	2.90 ± 0.08	64.3 ± 2.1	2.46 ± 0.29	1.15 ± 0.06	400 ± 41
EA–MPS15	15	7.27	3.12 ± 0.09	77.2 ± 1.6	2.88 ± 0.21	1.38 ± 0.03	536 ± 26
EA–MPS20	20	9.46	3.26 ± 0.07	68.3 ± 3.1	2.48 ± 0.15	1.26 ± 0.14	427 ± 94

[a] EA is the neat epoxyacrylate; EA–PS series are the epoxyacrylate composites filled with the pure silica; EA–MPS series are the epoxyacrylate composites filled with the surface-modified silica.

[b] The volume fractions of silica spheres were estimated according to the weight ratio of each component and the densities of epoxyacrylate matrix and silica spheres were 1.23 and 70 g/cm^3, respectively.

[c] Mean and standard deviation values calculated from five determinations.

the shape factor of the filler. The volume fraction (V_f) of silica spheres was estimated according to the weight ratio of each component and the material densities (epoxyacrylate matrix: 1.23 g/cm^3 and silica spheres: 70 g/cm^3). ζ is equal to 2 for the spherical particles used in the present study.

The results predicted by the Halpin–Tsai model were plotted as the solid line in Fig. 5, together with the measured moduli of the composites filled with different volume fractions of PS and MPS. The trend of the experimental data agrees with the prediction; however, the measured moduli of the EA–PS composites deviate significantly from the predicted line at higher volume fractions. The reason is that the Halpin–Tsai model assumes a per-
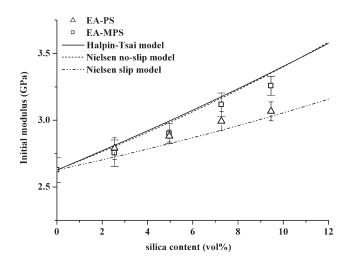

FIG. 5. The initial modulus of the epoxyacrylate composites versus volume fraction of silica spheres. Open symbols are the experimental data. The solid line represents the prediction from Halpin–Tsai model. The dashed lines are predictions using the Lewis–Nielsen model for no slip at the particle–matrix interface ($K_E = 2.167$) and for interfacial slippage ($K_E = 0.867$). EA–PS is the epoxyacrylate filled with PS spheres and EA–MPS is the epoxyacrylate filled with MPS spheres.

fect bonding between the particle and the matrix. This violates the fact that there is no chemical bonding between the silica spheres and the matrix in the EA–PS composites. Yet, the moduli of the EA–MPS samples are much closer to the predicted results, especially in the region of higher silica contents, within 7.27 and 9.46 vol%. This is because the MPS had vinyl functional groups on the surface that enabled chemical bonding between the particles and the matrix.

The effect of interfacial bonding can be considered further using the Lewis–Nielsen model [36] and the work of McGee and McCullough [37]. The modulus of the epoxyacrylate–silica composite can be predicted using:

$$E_c = \frac{1 + (k_E - 1)\beta V_f}{1 - \eta \mu V_f} E_m \qquad (3)$$

where k_E is the generalized Einstein coefficient, and β and μ are constants. $k_E = 2.5$ if there is no slippage and $k_E = 1.0$ if there is slippage at the interface between the particle and the matrix. Yet, Nielsen [38] has shown that the value of k_E is reduced when the Poisson's ratio (v) of the matrix is lower than 0.5. In the present study, $v = 0.35$ is taken, and hence the values of k_E are reduced by a factor of 0.867. Hence, $k_E = 2.167$ if there is no slippage, and $k_E = 0.867$ if there is slippage at interface between the particle and the matrix. The constant β takes into account the relative modulus of the particles and the matrix, and is given by

$$\beta = \frac{\left(\frac{E_f}{E_m} - 1\right)}{\left(\frac{E_f}{E_m} + (k_E - 1)\right)}. \qquad (4)$$

The value of μ depends on the maximum allowable volume fraction of particles, V_{max}, and can be calculated from

$$\mu = 1 + \frac{(1-V_{\mathrm{f}})}{V_{\max}}[V_{\max}V_{\mathrm{f}} + (1-V_{\max})(1-V_{\mathrm{f}})]. \quad (5)$$

Values of $V_{\max}$ have been published by Nielsen and Landel [39] for a range of particle shapes and types of packing. It will be shown later in the SEM pictures of the fractured surface of epoxyacrylate composites that the silica spheres appear to be nonagglomerated and randomly arranged in the matrix. Nielsen and Landel quoted a value of $V_{\max} = 0.632$ for such random-close packing, nonagglomerated spheres. This value was thus used in *Eq. 5*.

The predictions from the "no-slip" and "slip" Nielsen models are also shown in Fig. 5. The predictions of the Halpin–Tsai and the "no-slip" Nielsen models almost overlap with each other. The moduli of the EA–MPS composites are much closer to these prediction lines, indicating the presence of perfect bonding between the silica spheres and the matrix. In addition, it can be seen that reducing the adhesion between the particles and the matrix reduces the value of k_{E} and thus the predicted modulus. The experimental data of the EA–PS composites are somewhere between the predictions from the "no-slip" and "slip" Nielsen models and are closer to the prediction line from the "slip" Nielsen model. This indicates that there were still some weak interactions between the PS particles and the matrix.

Both ultimate tensile strength (σ_{b}) and elongation at break (ε_{b}) were found to increase with increasing the silica content, as summarized in Table 1. Both values reached their maxima in the EA–PS composites when 15 phr silica spheres (equivalent to 7.27 vol%) were added, and the calculated maximum relative improvements to the neat EA resin in the σ_{b} and ε_{b} were 1.91 and 1.70, respectively. In addition, the σ_{b} and ε_{b} of the EA–MPS composites were higher than those values of the respective EA–PS composites with the same added amount of silica. The reason is that the surface modification with MPTMS could enhance the dispersion of silica particles and provide chemical bonding between the silica particles and the matrix. The maximum values of σ_{b} and ε_{b} for the EA–MPS composite were also found with 15 phr of MPS spheres, and their relative improvements reached 2.22 and 2.03, respectively. With higher MPS content of 20 phr, both σ_{b} and ε_{b} of the composites began to decline. This is because slight aggregation occurred at this composition as proved in the SEM picture of the fracture surface of the composites, which will be discussed later.

Fracture Toughness and Fracture Surface

The SENB test was used to determine the fracture toughness, K_{Ic}, according to ASTM D5045. The value of the fracture energy, G_{Ic}, was then calculated using *Eq. 1*. A K_{Ic} value of 0.66 MPa-m$^{1/2}$ was obtained for the neat epoxyacrylate resin. The fracture toughness was found to increase by the addition of silica spheres, as summarized in Table 1. The increase was much higher for the system with MPS at the same added amount of silica spheres. For the epoxyacrylate composite with 15 phr MPS, a maximum value of 1.38 MPa-m$^{1/2}$ was observed. In other words, the fracture toughness increased by 109% by adding 15 phr MPS. Thus, strong interfacial bonding is advantageous for increasing fracture toughness. The fracture energy (G_{Ic}) of epoxyacrylate–silica composites calculated via *Eq. 1* also increased with silica content as summarized in Table 1. The stronger interfacial bonding in the EA–MPS is also responsible for the higher fracture energy as compared to the EA–PS. By adding 15 phr MPS, the fracture energy could increase by 270% from 145 to 536 J/m^2. For the same adding amount, the fracture energy of EA–PS was about 439 J/m^2. However, the K_{Ic} and G_{Ic} of the composite started to decrease when the silica content reached 20 phr which is believed owing to the slight aggregation of silica spheres.

The reason for the significant increase in toughness can be explained by the fracture behavior through the observation of fracture surface. As shown in Fig. 6a, the fracture surface of the neat epoxyacrylate is relatively smooth and featureless, which is typical of a brittle thermosetting polymer. There was no large-scale plastic deformation during fracture. Therefore, the fracture toughness of the neat epoxyacrylate was low and the K_{Ic} value was only 0.66 MPa-m$^{1/2}$. However, the addition of PS or MPS resulted in a rougher surface where the crack deflection and bifurcation were observed, as shown in Fig. 6b–d.

Johnsen et al. [14] have considered the toughening mechanisms induced by the silica nanoparticles in detail. The toughening mechanisms can be broadly categorized as on-plane processes (such as crack pinning or bowing and crack deflection) or off-plane processes (such as debonding and plastic void growth). Crack pinning occurs when the particles are larger than the crack-opening displacement, and it is identified by the presence of bowing lines on the fracture surface [40]. Under plane-strain conditions, the crack-opening displacement, δ_{tc}, can be calculated using the relationship [14]:

$$\delta_{\mathrm{tc}} = \frac{K_{\mathrm{Ic}}^2}{E\sigma_{\mathrm{y}}}(1-v^2) = \frac{G_{\mathrm{Ic}}}{\sigma_{\mathrm{y}}} \quad (6)$$

where σ_{y} is the yield stress of the matrix.

For the neat epoxyacrylate, the value of the crack-opening displacement calculated by using the data in Table 1 is 4.2 μm. For the epoxyacrylate–silica composite with the maximum toughness, that is, the one with 15 phr MPS, a value of $\delta_{\mathrm{tc}} = 6.9$ μm is obtained. It is thus clear that particles which are so much smaller than the crack-opening displacement are unlikely to cause crack pinning. Furthermore, the absence of bowed crack front markings on the fracture surfaces indicates that crack pinning is unlikely to be responsible for the observed increase in toughness.

It is well known that crack deflection by particles can lower the local crack-tip stress intensity factor and
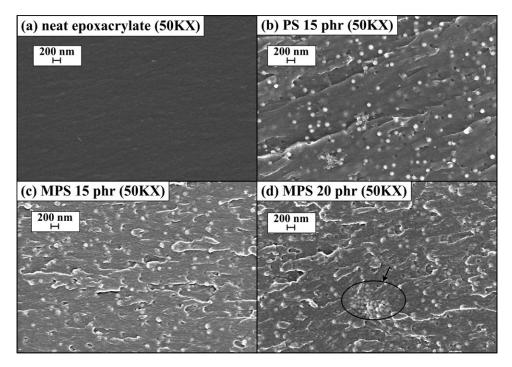
FIG. 6. SEM images of the fracture surface of (a) neat epoxacrylate, (b) epoxyacrylate composite with 15 phr PS, (c) epoxyacrylate composite with 15 phr MPS, and (d) epoxyacrylate composite with 20 phr MPS.

enhance fracture resistance. The crack deflection is owing to the tilt and twist of crack front when the crack propagation is resisted by the silica particles and hence the crack passes around the particle surface. This causes an increase in the total fracture surface area and also causes the crack to grow locally. The addition of MPS or PS resulted in a rougher surface, as shown in Fig. 6, indicates that crack deflection is one of the reasons for improving toughness.

Another possible reason for the increase of toughness could be the particle–matrix debonding followed by plastic void growth, in other words, energy consumption at the interface. Debonding is essential because it reduces the constraint at the crack tip and hence allows the matrix to deform plastically via a void growth mechanism. The particle–matrix debonding could be seen under a high magnification in Fig. 6b–d. This demonstrates the occurrence of the plastic void growth of the epoxy matrix initiated by debonding of silica spheres. However, some spherical voids with sharp boundary are also shown in Fig. 6b, indicating that the interfacial strength in the EA–PS was not as strong as that in the EA–MPS. Therefore, the improvement in fracture toughness in the EA–PS was not as high as that in the EA–MPS.

The irregular voids without clear boundary are shown in Fig. 6c–d for the EA–MPS composites, because the MPS surface had vinyl functional groups which could be bonded with the matrix. The perfect bonding between the MPS and the matrix enables the crack propagation through the matrix above or below the poles of the particles. Hence, the crack propagation path in the system with perfect particle/matrix adhesion is expected to be

longer than that with poor adhesion. Consequently, the fracture toughness increases with the crack propagation path. This may be another reason why the fracture toughness of the EA–MPS composite is higher than that of the EA–PS composite. Therefore, improving the bonding between the particle surface and the matrix could effectively increase the toughness.

Coefficient of Thermal Expansion and Glass Transition Temperature (T_g)

Generally, in a composite system, the expansion of the matrix is constrained owing to the presence of inorganic fillers [41]. Therefore, as summarized in Table 2, the coefficient of thermal expansions (CTEs) of composites below T_g (α_1) and above T_g (α_2) decreased with an increase in the silica content. The CTE decreased from 41 μm/m$^{\circ}$C for the neat epoxyacrylate to 30 μm/m$^{\circ}$C for the epoxyacrylate composite with 20 phr PS below T_g, and from 265 μm/m$^{\circ}$C to 210 μm/m$^{\circ}$C above T_g.

The glass transition temperature (T_g) of the cured composites could be determined by using both differential scanning calorimetry and thermal mechanical analysis. As clearly summarized in Table 2, the addition of PS only slightly decreased the glass transition temperature of the epoxyacrylate by 2°C from DSC and by 5°C from TMA. One possible reason is that the silica spheres induced a slight reduction in the crosslinking density of the polymer matrix. Preghenella et al. [42] also noticed a reduction in the glass transition temperature of the nanosilica-filled epoxies. They proposed that the nanosilica could cause a reduction in the crosslinking degree of the polymer matrix

TABLE 2. The glass transition temperature (T_g) and CTE of epoxyacrylate–silica composites filled with different silica contents.

Sample[a]	Silica content		T_g (°C)		CTE[b]	
	Weight (phr)	Volume (%)	DSC	TMA	α_1 (ppm/°C)	α_2 (ppm/°C)
EA	0	0	135.3	137.3	41.7	265.2
EA–PS5	5	2.55	133.5	135.1	32.8	261.4
EA–PS10	10	4.96	135.2	130.8	33.7	244.0
EA–PS15	15	7.27	135.6	133.7	33.6	220.7
EA–PS20	20	9.46	134.5	133.1	30.3	210.0
EA–MPS5	5	2.55	133.5	133.5	42.1	267.1
EA–MPS10	10	4.96	128.7	131.6	42.7	253.5
EA-MPS15	15	7.27	127.6	128.8	36.2	236.2
EA–MPS20	20	9.46	123.0	123.3	31.7	223.9

[a] EA is the neat epoxyacrylate; EA–PS series are the epoxyacrylate composites filled with the pure silica; EA–MPS series are the epoxyacrylate composites filled with the surface-modified silica.

[b] α_1, linear CTE bellow T_g; α_2, linear CTE above T_g.

by effectively preventing the complete curing of the epoxy.

It is more obvious that the addition of MPS decreased the glass transition temperature of the epoxyacrylate matrix. The T_g decreased from 135°C for the neat epoxyacrylate to 123°C for the EA–MPS with 20 phr MPS. It indicates that in addition to the reduction in the crosslinking density of the polymer matrix by the silica spheres, the MPTMS on the surface of MPS could increase the chain mobility of the epoxy resin in the composite.

CONCLUSIONS

Highly uniform silica spheres were prepared from the hydrolysis and condensation reaction of TEOS in the ammonia/ethanol solution. The surface of the spheres was further modified by reaction with MPTMS to have vinyl functional group. It was found that the MPTMS could inhibit the growth of particles and decrease the yield of submicron particles. The results revealed that the epoxyacrylate–silica composites had higher tensile mechanical properties and fracture toughness than the neat epoxyacrylate. In addition, the increase was larger for the epoxyacrylate filled with MPS silica spheres than the system with PS. This is because there was chemical bonding between the MPS silica spheres and the matrix, thus providing stronger interfacial strength. By adding 15 phr MPS into the epoxyacrylate, the K_{Ic} and G_{Ic} could be increased by 109 and 270%, respectively. The toughening mechanisms as evidenced from the observation of fracture surface include crack deflection and particle–matrix debonding. The micrographs showed that the perfect bonding between the MPS and the matrix leaded to the increase in the crack propagation path and the absorption of energy in particle debonding, which could effectively increase the fracture toughness.

REFERENCES

1. R. Mezzenga, L. Boogh, and J.-A.E. Manson, *Compos. Sci. Technol.*, **61**, 787 (2001).

2. M. Imanaka, Y. Takeuchi, Y. Nakamura, A. Nishimura, and T. Iida, *Int. J. Adhes. Adhes.*, **21**, 389 (2001).

3. C.A. May and Y. Tanaka, *Epoxy Resins: Chemistry and Technology*, Marcel Dekker, New York , **794** (1988).

4. S.K. Bhattacharya and R.R. Tummala, *Microelectron. J.*, **32**, 11 (2001).

5. Y. Li and C.P. Wong, *Mater. Sci. Eng. R Rep.*, **51**, 1 (2006).

6. D.K. Chattopadhyay, S.S. Panda, and K.V.S.N. Raju, *Prog. Org. Coat.*, **54**, 10 (2005).

7. G. Yang, H. Liu, L. Bai, M. Jiang, and T. Zhu, *Micropor. Mesopor. Mat.*, **112**, 351 (2008).

8. C. Decker, T. Nguyen Thi Viet, D. Decker, and E. Weber-Koehl, *Polymer*, **42**, 5531 (2001).

9. J. Lange and J. A. E. Manson, *Polymer*, **37**, 5859 (1996).

10. Y.-J. Park, H.-J. Kim, D.-S. Park, and I.-K. Sung, *Eur. Polym. J.*, **46**, 1642 (2010).

11. M.L. Auad, P.M. Frontini, J. Borrajo, and M.I. Aranguren, *Polymer*, **42**, 3723 (2001).

12. P. Rosso, L. Ye, K. Friedrich, and S. Sprenger, *J. Appl. Polym. Sci.*, **100**, 1849 (2006).

13. Y.L. Liang and R.A. Pearson. *Polymer*, **50**, 4895 (2009).

14. B.B. Johnsen, A.J. Kinloch, R.D. Mohammed, A.C. Taylor, and S. Sprenger, *Polymer*, **48**, 530 (2007).

15. S. Kang, S. Hong, C.R. Choe, M. Park, S. Rim, and J. Kim, *Polymer*, **42**, 879 (2001).

16. K.S. Chan, Y.D. Lee, D.P. Nicolella, B.R. Furman, S. Wellinghoff, and R. Rawls, *Eng. Fract. Mech.*, **74**, 1857 (2007).

17. A. Hartwig, M. Sebald, D. Pütz, and L. Aberle, *Macromol. Symp.*, **221**, 127 (2005).

18. F. Bondioli, V. Cannillo, E. Fabbri, and M. Messori, *J. Appl. Polym. Sci.*, **97**, 2382 (2005).

19. E. Bugnicourt, J. Galy, J.F. Gerard, and H. Barthel, *Polymer*, **48**, 1596 (2007).

20. C.Y. Chen, C.K. Huang, S.P. Lin, J.L. Han, K.H. Hsieh, and C.P. Lin, *Compos. Sci. Technol.*, **68**, 2811 (2008).

21. Y.-C. Su, L.-P. Cheng, K.-C. Cheng, and T.-M. Don, *Mater. Chem. Phys.*, **132**, 540 (2012).

22. W. Stöber, A. Fink, and E. Bohn, *J. Colloid Interface Sci.*, **26**, 62 (1968).

23. P. Hajji, L. David, J.F. Gerard, J.P. Pascault, and G. Vigier, *J. Polym. Sci. B Polym. Phys.*, **37**, 3172 (1999).

24. A. Fidalgo and L.M. Ilharco, *J. Non-Cryst. Solids*, **283**, 144 (2001).

25. E. Lippmaa, M. Mägi, A. Samoson, G. Engelhardt, and A.R. Grimmer, *J. Am. Chem. Soc.*, **102**, 4889 (1980).

26. S.K. Young, W.L. Jarrett, and K.A. Mauritz, *Polymer*, **43**, 2331 (2002).

27. M.P.J. Peeters, W.J.J. Wakelkamp, and A.P.M. Kentgens, *J. Non-Cryst. Solids*, **189**, 77 (1995).

28. M.C. Brochier-Salon, P.A. Bayle, M. Abdelmouleh, S. Boufi, and M.N. Belgacem, *Colloids Surf. A*, **312**, 83 (2008).

29. F. Bauer, V. Sauerland, H.J. Glasel, H. Ernst, M. Findeisen, E. Hartmann, H. Langguth, B. Marqardt, and R. Mehnert, *Macromol. Mater. Eng.*, **287**, 546 (2002).

30. A. Van Blaaderen and A. Vrij, *J. Colloid Interface Sci.*, **156**, 1 (1993).

31. Y.S. Chung, M.Y. Jeon, and C.K. Kim, *Macromol. Res.*, **17**, 37 (2009).

32. J. W. Kim, L. U. Kim, and C. K. Kim, *Biomacromolecules*, **8**, (2007).

33. I.A.M. Ibrahim, A.A.F. Zikry, and M.A. Sharaf, *J. Amer. Sci.*, **6**, 985 (2010).

34. J. Cho, M.S. Joshi, and C.T. Sun, *Compos. Sci. Technol.*, **66**, 1941 (2006).

35. J.C. Halpin and J.L. Kardos. *Polym. Eng. Sci.*, **16**, 344 (1976).

36. T.B. Lewis and L.E. Nielsen, *J. Appl. Polym. Sci.*, **14**, 1449 (1970).

37. S. McGee and R.L. McCullough, *Polym. Compos.*, **2**, 149 (1981).

38. L.E. Nielsen, *J. Compos. Mater.*, **2**, 120 (1968).

39. L.E. Nielsen and R.F. Landel, *Mechanical Properties of Polymers and Composites*, 2nd ed., Marcel Dekker, New York (1994).

40. A.J. Kinloch, D.L. Maxwell, and R.J. Young, *J. Mater. Sci.*, **20**, 416 (1985).

41. T.-H. Ho and C.-S. Wang, *J. Appl. Polym. Sci.*, **51**, 2047 (1994).

42. M. Preghenella, A. Pegoretti, and C. Migliaresi, *Polymer*, **46**, 12065 (2005).